*Cerebral Cortex*, September 2018;28: 3192–3203

**doi: 10.1093/cercor/bhx191**
Advance Access Publication Date: 9 August 2017
Original Article

ORIGINAL ARTICLE

# Disorganized Patterns of Sulcal Position in Fetal Brains with Agenesis of Corpus Callosum

Tomo Tarui[1,2,5,6], Neel Madan[7], Nabgha Farhat[1,2], Rie Kitano[5], Asye Ceren Tanritanir[1,2], George Graham[8], Borjan Gagoski[1,3], Alexa Craig[9], Caitlin K. Rollins[4], Cynthia Ortinau[10,11], Vidya Iyer[5], Rudolph Pienaar[1,3], Diana W. Bianchi[12], P. Ellen Grant[1,2,3] and Kiho Im[1,2]

[1]Fetal Neonatal Neuroimaging and Developmental Science Center, Boston Children's Hospital, Harvard Medical School, Boston, MA 02115, USA, [2]Division of Newborn Medicine, Boston Children's Hospital, Harvard Medical School, Boston, MA 02115, USA, [3]Department of Radiology, Boston Children's Hospital, Harvard Medical School, Boston, MA 02115, USA, [4]Department of Neurology, Boston Children's Hospital, Harvard Medical School, Boston, MA 02115, USA, [5]Mother Infant Research Institute, Tufts Medical Center, Tufts University School of Medicine, Boston, MA 02111, USA, [6]Department of Pediatrics, Tufts Medical Center, Tufts University School of Medicine, Boston, MA 02111, USA, [7]Department of Radiology, Tufts Medical Center, Tufts University School of Medicine, Boston, MA 02111, USA, [8]Department of Obstetrics and Gynecology, Tufts Medical Center, Tufts University School of Medicine, Boston, MA 02111, USA, [9]Department of Pediatrics, Maine Medical Center, ME 04102, USA, [10]Department of Pediatrics Newborn Medicine, Brigham and Women's Hospital, Harvard Medical School, Boston, MA 02115, USA, [11]Department of Pediatrics, Washington University School of Medicine, St. Louis, MO 63110, USA and [12]Medical Genetics Branch, National Human Genome Research Institute, Bethesda, MD 20892, USA

Address correspondence to Kiho Im, Boston Children's Hospital, 1 Autumn Street, Boston, MA 02115, USA. Email: Kiho.Im@childrens.harvard.edu

## Abstract

Fetuses with isolated agenesis of the corpus callosum (ACC) are associated with a broad spectrum of neurodevelopmental disability that cannot be specifically predicted in prenatal neuroimaging. We hypothesized that ACC may be associated with aberrant cortical folding. In this study, we determined altered patterning of early primary sulci development in fetuses with isolated ACC using novel quantitative sulcal pattern analysis which measures deviations of regional sulcal features (position, depth, and area) and their intersulcal relationships in 7 fetuses with isolated ACC (27.1 ± 3.8 weeks of gestation, mean ± SD) and 17 typically developing (TD) fetuses (25.7 ± 2.0 weeks) from normal templates. Fetuses with ACC showed significant alterations in absolute sulcal positions and relative intersulcal positional relationship compared to TD fetuses, which were not detected by traditional gyrification index. Our results reveal altered sulcal positional development even in isolated ACC that is present as early as the second trimester and continues throughout the fetal period. It might originate from altered white matter connections and portend functional variances in later life.

**Key words:** agenesis of corpus callosum, fetus, prenatal diagnosis, quantitative MRI, sulcal development

## Introduction

The corpus callosum is the largest interhemispheric white matter connection in the human brain, consisting of more than 190 million axons connecting the 2 hemispheres of the brain (Bloom and Hynd 2005). The corpus callosum develops between 11 and 15 weeks of gestation with a process that is complex and involves multiple cellular and molecular events (Richards et al. 2004). Prenatal disruption of one or more of these events can lead to complete or partial agenesis of the corpus callosum (ACC) (Paul et al. 2007; Kasprian et al. 2013). ACC is one of the most commonly occurring brain malformations found in 2–3% of individuals with intellectual disability (Jeret et al. 1987). While syndromic or complex ACC, refers to callosal agenesis as one of the features of genetic syndromes or association with other central nervous system (CNS) or extra-CNS malformations, likely associates with more severe neurodevelopmental outcome, people with "isolated" ACC without apparent such associations have a broad spectrum of neurodevelopmental manifestations in intellectual and behavioral skills (Siffredi et al. 2013). This has been one of the major challenges in predicting the outcomes of affected individuals with isolated ACC at younger ages, especially during fetal life (Fratelli et al. 2007; Chadie et al. 2008; Ghi et al. 2010; Mangione et al. 2011). Currently, there is no anatomical basis upon which to predict neurodevelopmental outcomes for fetuses with isolated ACC when no additional CNS or extra-CNS malformations are recognized.

We hypothesized that ACC and associated aberrant white matter organization may influence cortical folding patterns. The primary sulcal folding pattern in the human cerebral cortex is prenatally determined and has been hypothesized to be associated with organization of cortical functional areas and their white matter connections (Van Essen 1997; Klyachko and Stevens 2003; Fischl et al. 2008; Sun and Hevner 2014). Disrupted sulcal patterns caused by defective neurodevelopmental processes have been observed in many brain malformations and psychiatric/neurological disorders (Molko et al. 2003; Nakamura et al. 2007; Cykowski et al. 2008; Kim et al. 2008; Shim et al. 2009; Barkovich et al. 2012; Im et al. 2013, 2016; Bae et al. 2014). Second to third trimester fetuses with ACC also showed delayed maturation or abnormal morphology of sulci (Tang et al. 2009; Warren et al. 2010). In these previous ACC studies, sulcal patterns were measured by qualitative visual scoring of sulcal maturities rather than quantitative indices.

In prior work, a quantitative sulcal pattern analysis technique—similarity index (SI)-based sulcal pattern analysis method—was developed that is complementary to qualitative methods (Im et al. 2011, 2013, 2016). Our analytical method enables global examination of primary sulcal patterning in three-dimensional (3D) space, which is difficult to assess by qualitative visual inspection of 2-dimensional images. Our approach allows not only the comparison of regional features of sulcal folds (position, depth, and size), but also their intersulcal geometric and topological relationships (sulcal organization and arrangement). This method has proven useful for quantification and discrimination of abnormal sulcal patterns in polymicrogyria (Im et al. 2013; Bae et al. 2014). Another study showed atypical global sulcal patterns in parieto-temporal and occipito-temporal cortical regions in children with developmental dyslexia (Im et al. 2016) where decreased fractional anisotropy in diffusion tensor MR imaging suggests altered white matter organization (Rimrodt et al. 2010; Vandermosten et al. 2012). Recently, atypical early sulcal pattern was revealed in human fetuses with brain abnormalities using this method (Im et al. 2017). To our knowledge, cortical folding patterns associated with ACC have not been previously measured.

The aim of this study was to use our quantitative sulcal pattern analysis technique to measure the patterns of early sulcal folding in fetal brains with isolated ACC. Both partial and complete isolated ACC was analyzed as they both have equivalent outcomes and challenges to predict outcome prenatally (D'Antonio et al. 2016). We hypothesized that the sulcal patterns measured with this relatively novel method would be abnormal as atypical patterns are likely to originate due to disrupted and/or rewired white matter connections. In addition, the results of sulcal pattern analysis were compared to an established metric, the gyrification index (GI), which provides a measure of the overall amount of cortical folding. The GI has been widely used to quantify folding in human cortical development (Zilles et al. 1988; Armstrong et al. 1995; Clouchoux et al. 2013; Lefevre et al. 2015) and is thought to be sensitive to detect developing cerebral abnormalities (Shimony et al. 2016).

## Materials and Methods

### Subjects

The study was approved by the Institutional Review Boards of all participating institutions. MR images from fetuses with isolated partial and complete ACC were identified from (1) a retrospective search of existing patient data at the Boston Children's Hospital (BCH) and (2) prospective recruitment into a fetal case control study at the Tufts Medical Center (TMC) and Maine Medical Center (MMC) in the United States of America. In this study, isolated ACC cases were recruited if callosal agenesis is partial or complete and without features of genetic syndromes nor association with other CNS or extra-CNS malformations. ACC with colpocephaly is included as it is often a secondary finding. Pregnant women with healthy fetuses were recruited as typically developing (TD) fetuses and offered fetal MRI scans that were used as controls. The consent process was waived for data collected retrospectively. Written consent was obtained from pregnant women recruited prospectively. Inclusion of patient data in this study was based on the following criteria: gestational age from 22 to 32 gestational weeks (GW); ACC; no obvious associated CNS malformations. We searched for cases that were clinically diagnosed with isolated ACC based on the fetal MRI. The clinical imaging diagnoses were confirmed by a pediatric neurologist (T.T.) and 2 neuroradiologists (N.M. and P.E.G.). Images were excluded if significant motion or other artifacts that degraded image quality were present.

Healthy control subjects were identified and recruited at 2 institutions: at BCH, pregnant women referred to the Advanced Fetal Care Center due to a family history of congenital heart disease but for whom fetal echocardiogram was normal while at TMC, TD fetuses were recruited by approaching healthy pregnant women with uncomplicated pregnancies from the Obstetric clinic. Inclusion criteria for controls were: maternal age 18–45 years; gestational age 22–32 weeks. Of note, gestational age of the subjects was determined per standard care at obstetric clinics utilizing sonographic biometric measurements of the fetuses in the first and second trimester (crown–rump length, biparietal diameter, etc.). We excluded multiple gestation pregnancies, fetuses with dysmorphic features on ultrasound examination, other brain malformations or brain lesions, known chromosomal abnormalities, other identified organ anomalies, and known congenital infections. We also

excluded subjects as healthy controls if the fetal MRI identified any abnormality.

## MRI Acquisition and Identification of Sulcal Basins on the Cortical Plate Surface

Fetal brains were scanned using a single shot fast spin echo T2 technique (HASTE, Half-Fourier Acquisition Single- Shot Turbo Spin-Echo, on Siemens; SSTSE, single shot turbo spin echo on Philips; SSFSE, single shot fast spin echo on GE). The MRI sequence was obtained on a Siemens 3 T scanner (BCH), Phillips 1.5 T scanner (TMC), or GE 1.5 T scanner (MMC). The following sequence was used for each subject: time repetition = ~1.5 s (BCH) or 12.5 s (TMC, MMC), time echo = 120 ms (BCH) or 180 ms (TMC, MMC), field of view = 256 mm (TMC, BCH) or 360–420 mm (MMC), in-plane resolution = 1 mm, slice thickness = 2–3 mm. The HASTE acquisition was acquired at least three times in different orthogonal orientations. In addition to these, 3 to 12 HASTE scans (depending on the severity of the motion artifacts) orientated at ~30–45° relative to the original three orthogonal scans were acquired for reliable image postprocessing. At initial review, MRI studies without severe motion or other artifacts in the brain region were included in the study.

Fetal head motion correction and isotropic high-resolution volume reconstruction (voxel size: 0.75 × 0.75 × 0.75 [mm]) were performed from the multiple scans (Kuklisova-Murgasova et al. 2012). The volume images of each subject were manually aligned along the anterior and posterior commissure (AC–PC) points using AFNI (afni.nimh.nih.gov/afni), which needs definition of AC superior edge and posterior margin points, PC inferior edge point, and 2 other points in the interhemispheric mid-sagittal plane (Cox 2012). The cortical plate was semiautomatically segmented using FreeView (surfer.nmr.mgh.harvard.edu). The cortical plate was first automatically segmented on each slice using intensity value ranges and then manually corrected by examining the volume image on orthogonal views. The inner volume of the cortical plate was binarized and smoothed using a 3 × 3 × 3 mean filter for the reconstruction of smooth surface models that are less susceptible to noise. The 3D inner cortical plate surface was then reconstructed using the isosurface function with the isovalue of 0.5 from the Matlab software (Fig. 1) (Im et al. 2017). Although small folds of the similar size with a voxel might be eliminated, our smoothing was necessary and effective to avoid noise and voxelized representation of the brain surface.

Early developing sulcal catchment basins were identified and used for sulcal pattern analysis because they are relatively invariant between subjects and are hypothesized to relate to functional areas and activations (Derrfuss et al. 2009; Im et al. 2010). Sulcal catchment basins are substructures decomposed from 1 large sulcus and defined to be concavities on the cortical surface that are separated by convex ridges (Lohmann and von Cramon 2000; Im et al. 2010). Mean curvature and depth maps on a cortical surface model were generated using the FreeSurfer software (surfer.nmr.mgh.harvard.edu). The curvature map was smoothed using the surface-based heat kernel smoothing with a full-width half-maximum value of 5 mm (Chung et al. 2005). Sulcal basins were automatically identified using a watershed algorithm based on the smoothed curvature map (Im et al. 2010, 2011, 2013, 2016). To prevent over-extraction of the segments, segment merging was performed using the normalized area of the basin (sulcal basin area/whole cortical surface area) with a threshold of 0.001. When 2 or more sulcal basins met at a ridge point in the watershed process, the sulcal basin smaller than a threshold (0.001) was merged into the adjacent sulcal basin. A minimum bounding box for a given surface model was created, and an average 3D relative position ($x$: left–right [0–1], $y$: posterior–anterior [0–1], $z$: inferior–superior [0–1]) was calculated for each sulcal basin. We also computed the normalized surface area ($s$) and mean sulcal depth ($d$) of sulcal basins to capture their geometry (Im et al. 2017).

We used 9 fetal brain templates from 23 to 31 GW as a reference to assess normality/abnormality of individual sulcal patterns, which were previously published (brain-development.org/brain-atlases) (Serag et al. 2012). The cortical plate surface extraction and identification and geometric measurements of sulcal basins from the fetal templates were performed using the same process. The sulcal sets of all 9 fetal brain templates were combined (Fig. 2).

## SI-Based Quantitative MRI Analysis: Sulcal Pattern Matching and Measurement of the Sulcal Pattern Similarity to the Normal Templates

Each individual fetal brain was quantitatively compared with the template brains and the sulcal pattern similarities to the templates were measured and examined for both the TD and ACC groups. For individual and template brains, 2 features of sulcal basins were determined: the local sulcal features (feature vector $F(i) = (x_i, y_i, z_i, s_i, d_i)$: 3D position, area, and depth of sulcal basin $i$) and also the intersulcal geometric relationships, $F(i) - F$

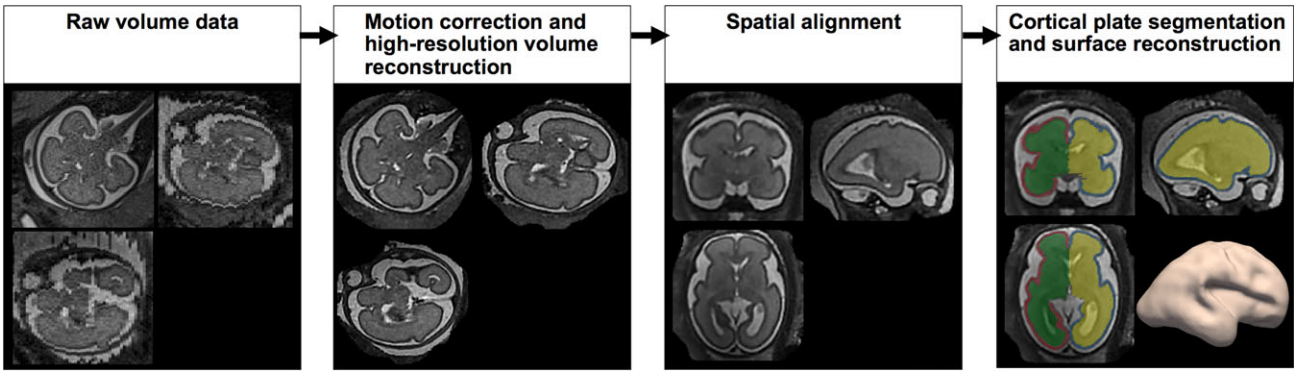


**Figure 1.** Processing fetal MRI for surface analysis. Raw volume data of fetal MRI is processed with motion correction and high-resolution volume reconstruction to reconstruct 3D fetal brain image. Reconstructed image is spatially aligned using anterior and posterior commissures as the landmark. Cortical plate of fetal brain is then segmented using Freeview. Segmentation data is used to reconstruct cortical plate surface.

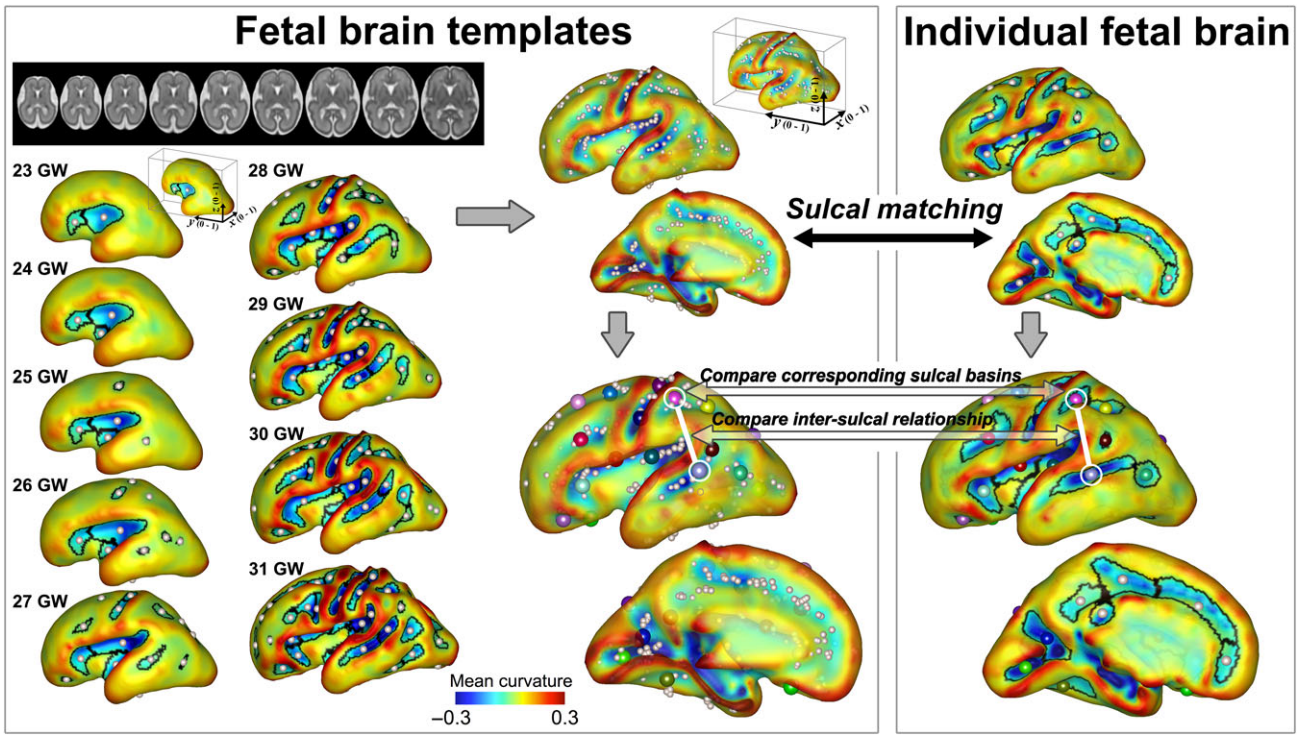


**Figure 2.** Identification and pattern analysis of sulcal basins. Sulcal basins of the individual fetal brain are identified on the cortical plate surface and optimally matched and compared with the set of sulcal folds generated from 9 fetal brain templates (23–31 GW). The spheres with the same color represent the matched corresponding sulcal basins between the templates and individual brain. Sulcal pattern similarity to the templates is measured for the individual brain.

$(u) = (x_i - x_u, y_i - y_u, z_i - z_u, s_i - s_u, d_i - d_u)$, in the left and right whole hemispheres (Im et al., 2011). The individual sulcal set was optimally matched with the combined set of 9 template fetal brains by having the minimum difference of the features between them. Since spatio-temporal patterns of sulcal folding are variable across individuals and fetuses with ACC may show delayed sulcal development or more variable sulcal patterns, we employed the sulcal set of all template brains in an unbiased manner for sulcal pattern matching and similarity measure rather than using specific template of similar ages with an assumption. Their SI was computed using a spectral matching technique (Leordeanu and Hebert 2005; Im et al. 2011) (Fig. 2). For each fetus, the patterns of sulcal similarity to the normal templates ranged from 0 to 1, reflecting the deviation from the normal sulcal pattern (Im et al. 2013, 2016, 2017). However, sulcal basins on the cingulate cortical area were excluded from the SI measurement because the cortical plate surfaces from several ACC cases showed anatomically meaningless folding on the medial area due to the absence of corpus callosum and associated absence of the cingulate gyrus. Various weighting of geometric features can be used for the SI measurement in this method. After measuring the SI with all three features (position, area, and depth), we further calculated SI only using each individual feature by setting all weights of the other features to 0 to evaluate their relative importance on the sulcal pattern similarity. See Im et al. 2011 for a more detailed explanation of the method for sulcal pattern matching and SI measurement.

As explained above, we aligned the cortical surface along the AC–PC line to use the position information of the sulcal basin. Although this is not a perfect spatial normalization, by defining corresponding regions and controlling for different brain size between individuals, re-orientation using the AC–PC line was considered sufficient for measuring the scale-free value of the relative position. However, because identification of the AC–PC points might be incomplete due to a low-effective resolution of fetal MRI and their locations might be different or abnormal in ACC, some brains might be more rotated to a downward or upward position along the *x*-axis (left–right axis), that is on the sagittal view, which could affect the sulcal position. It is easy to find the interhemispheric mid-sagittal plane and if we define anatomical points on that plane, the fetal brain is aligned well along *y*- and *z*-axes (on the coronal and axial views). Accordingly, we rotated the 3D position from –10 to 10 degrees along the *x*-axis (1 degree at a time) and measured sulcal pattern similarities for each position. The 1 sulcal set that showed the highest positional similarity to the templates, that was considered to show the most appropriate spatial alignment, was chosen for the following analysis. If the brain is aligned as described above, the relative sulcal positions defined by the bounding box capturing the brain are not affected by abnormal AC–PC anatomy.

Moreover, we separately measured the similarities by comparing the matched corresponding sulcal regions and the intersulcal relationships respectively between individual and template brains (Im et al. 2011) (Fig. 2). A simple example is provided in Supplementary Figure 1. In particular, examination of the similarity of intersulcal relationships is biologically and methodologically important as it can characterize and compare the intrinsic sulcal pattern that is minimally affected by overall brain size, shape, and orientation as well as global shift of sulcal folding.

## Three-dimensional GI

A global GI measures the complexity of cortical surface folding, which reflects the progression of gyrus formation in developing brain. The GI is defined as the ratio between the areas of the

cortical surface and its convex hull in 3D (Zilles et al. 1988; Schaer et al. 2008). The outer hull surface (which wraps the cortical plate surface) was defined by a 3D morphological closing operation using a 15 mm diameter sphere to close the sulcal folding (Schaer et al. 2008). It was created from the binary closed volume using the isosurface function. The 3D global GI was calculated from the inner cortical plate surface and outer hull surface in the left and right cerebral hemispheres in our cohort.

### Statistical Group and Individual Analysis

First, to test if age distribution was statistically matched between TD and ACC groups, an independent sample *t*-test was performed on gestational age. Group differences in sex ratio were assessed using a Fisher's exact test. The sulcal pattern similarities to the templates and GI were compared between TD fetuses and fetuses with ACC using an independent sample *t*-test. The GI is significantly associated with age in the fetal period (Zilles et al. 1988; Armstrong et al. 1995; Clouchoux et al. 2013; Lefevre et al. 2015). To test if the differences in the slopes of the GI change according to age between TD and ACC, the interaction effect between group and age was examined using a regression model ($Y = b_0 + b_1\text{group} + b_2\text{age} + b_3\text{group}\times\text{age} + e$, statistical test for $b_3$). Group differences of the sulcal pattern similarities to the normal templates were tested with the 4 different feature sets (combined feature, 3D position, sulcal area, and sulcal depth) for the left and right hemispheres separately. In all group difference tests of the sulcal pattern similarities, false discovery rate control was used to correct for multiple comparisons at a $q$-value of 0.05 (Benjamini and Hochberg 1995; Genovese et al. 2002).

Second, to illustrate the deviation of each ACC case in comparison with the natural distribution of sulcal pattern variation in TD fetuses, the SI of each ACC case was plotted onto the distribution of similarities in TD fetuses. We also counted the number of TD subjects with a lower SI and expressed that value as the ratio to the total number of TD subjects (histogram ranking), which ranged from 0 to 1. It is equivalent to a "percentile" and maps each fetus with ACC against the normal distribution for fetuses with TD. If a fetus with ACC showed a ratio of 0, it meant there was complete deviation from the distribution of TD fetuses.

## Results

### Subjects

Nine ACC and 23 TD fetuses were identified or recruited, but 2 ACC and 6 TD MRI data were excluded due to poor image quality and serious head motion in the fetal MRIs, which could not be sufficiently processed to reconstruct high-resolution volume and yield accurate fetal brain surfaces. As a result, 24 fetal brains were analyzed including 7 fetuses with isolated ACC and 17 TD fetuses. The gestational ages of the MRI studies (ACC, TD; mean ± SD (range)) were, respectively, 27.1 ± 3.8 (22.0–31.4) and 25.7 ± 2.0 (22.4–29.6) GW ($P = 0.24$, *t*-test). Fetal sex (female ACC 57.1%, TD 64.7%, $P = 1.00$, Fisher's exact test) and maternal age (28.3 ± 4.3, 30.4 ± 4.2, $P = 0.28$, *t*-test) were not significantly different between fetuses with ACC and TD. Following clinical MRI review, ACC cases were considered to be "isolated" ACC, without other CNS malformations. Four cases were complete ACC while three were partial ACC. All subjects were processed for motion correction, volume reconstruction, and AC–PC alignment. Based on segmentation data obtained using FreeView, the 3D inner cortical plate surface reconstruction and sulcal basins identification were successfully performed.

### Cerebral Anatomy of Isolated Agenesis of Corpus Callosum

Anatomy of isolated ACC and reconstructed cerebral surface was reviewed (Supplementary Fig. 2*a*–*c* and Fig. 3). As reported in former studies, anterior horns of lateral ventricles have vertical and parallel orientation (Supplementary Fig. 2*a*). Six cases had colpocephaly as early as 22 GW (Supplementary Fig. 2*b*). One case had mild ventriculomegaly but not typical colpocephaly (ACC5). In all 7 cases, both anterior (arrow) and posterior (data not shown) were identified (Supplementary Fig. 2*a*).

Although, no apparent associated CNS malformations were identified after reconstructing surface, visual presentation of primary fissures and sulci were somewhat different. Formation of Sylvian fissures appear to be shallower in fetuses with ACC compared to the TD fetuses (Supplementary Fig. 2*a*, *b* & Fig. 3), though it was not consistent.

### Group Comparison of Sulcal Pattern Between Agenesis of Corpus Callosum and TD Fetal Brains

The second and third trimester brains of fetuses with ACC had significantly different sulcal patterns in both left and right hemispheres compared to TD fetuses at a 0.05 level of corrected *P*-values. Table 1 summarizes statistical analysis of sulcal pattern similarity between TD and ACC groups with different feature sets such as sulcal position, sulcal basin area, sulcal basin depth, and combination of all of them. The analyses test these features as a whole, between corresponding sulci and intersulcal relationship. In all analyses, absolute sulcal position, and intersulcal positional relationship was significantly different between ACC and TD groups.

The differences were significant, when either whole pattern of sulcation (left $P = 0.0017$ and right $P = 0.0037$) or intersulcal relationships (left $P = 0.0009$ and right $P = 0.0059$) were compared, in all combined three sulcal features (3D sulcal position, area, and depth of sulcal basin) in both hemispheres. In the right hemisphere, combined 3 sulcal features were also different between corresponding sulcal regions but not in the left hemisphere (left $P = 0.3351$ and right $P = 0.0008$). The analyses also looked at each of these three features. Among these features, the 3D positions of sulci were different between ACC and TD in either analytical method, in whole pattern of sulcation (left $P < 0.0001$ and right $P = 0.0003$), in corresponding sulcal regions (left $P < 0.0001$ and right $P < 0.0001$) and in intersulcal relationships (left $P < 0.0001$ and right $P = 0.0003$) (Fig. 4, Table 1). There were no significant differences in sulcal basin area and sulcal depth between corresponding sulcal regions or intersulcal relationships. Therefore, absolute and relative position of the sulci led the significantly different sulcal pattern in the second trimester fetal brain with ACC compared to TD fetuses.

Figure 3 shows the cortical plate surfaces, sulcal basins identification, and the sulcal pattern similarities to the templates in all 7 ACC fetal brains and 9 TD fetal brains in age range from 22 to 31 GW. Spatial arrangement and position of sulcal basins in ACC brains appeared to be atypical compared with both individual TD brains (Fig. 3) and the template brains (Fig. 2), resulting in a low sulcal position SI.

### Individual Analysis of Sulcal Pattern in Agenesis of Corpus Callosum

Next, we examined whether the similarity of each fetus with ACC was outside the normal range by measuring its relative

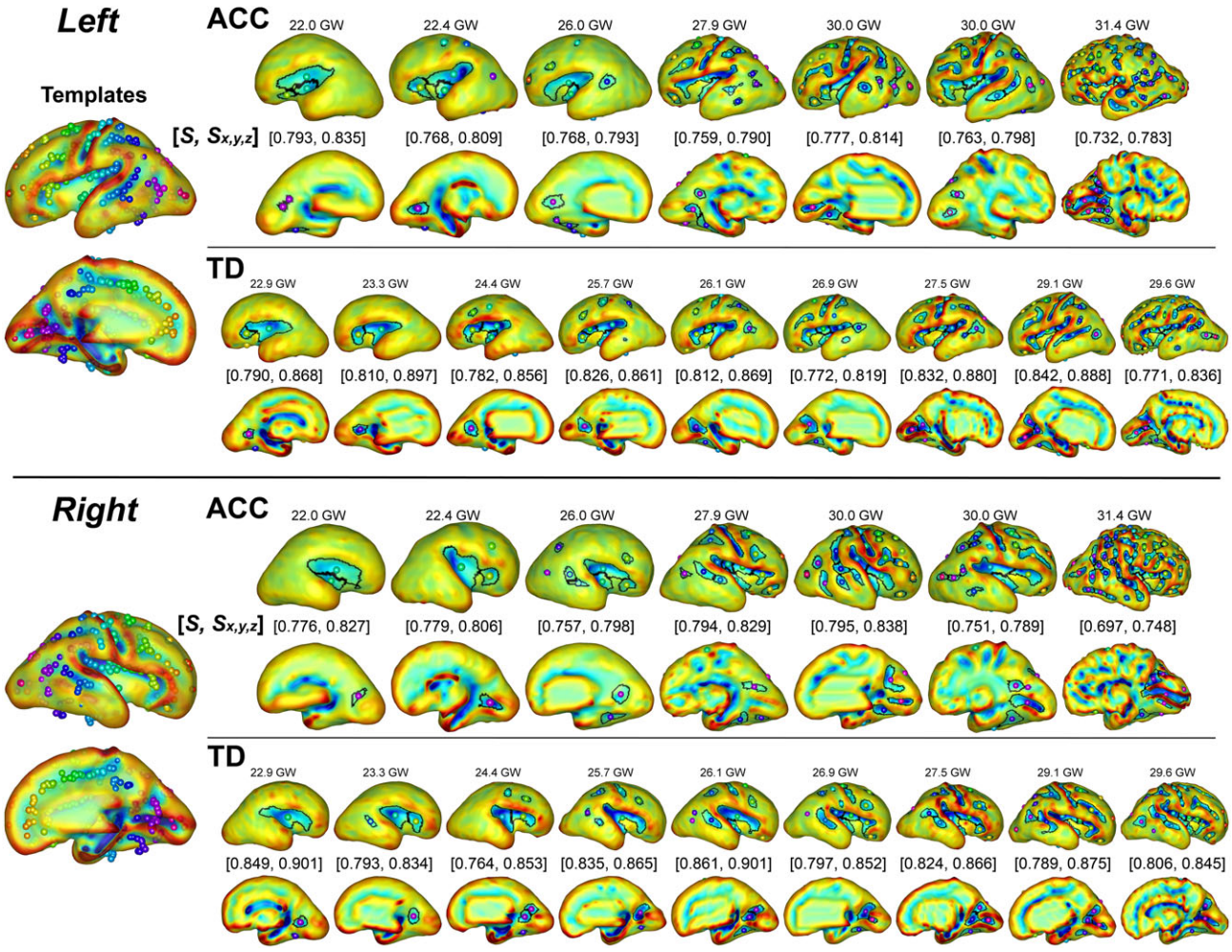


**Figure 3.** Sulcal basin identification on the cortical plate surface and sulcal pattern similarities to the templates with combined 3 features (S) and 3D position ($S_{x,y,z}$) in 7 ACC and 9 TD fetuses ranged from 22 to 31 GW. The ACC fetal brains show low sulcal pattern similarity values compared to TD fetal brains. The spheres with the same color represent the matched corresponding sulcal basins between the templates and individual brain.

**Table 1** Statistical analysis of sulcal pattern similarity between TD and ACC groups with different feature sets

| | Left hemisphere | | | Right hemisphere | | |
|---|---|---|---|---|---|---|
| | TD | ACC | P-value | TD | ACC | P-value |
| | Comparison of whole pattern | | | Comparison of whole pattern | | |
| Combined features | 0.811 (0.031) | 0.766 (0.019) | 0.0017* | 0.809 (0.030) | 0.764 (0.034) | 0.0037* |
| 3D position | 0.866 (0.030) | 0.803 (0.018) | <0.0001** | 0.859 (0.027) | 0.805 (0.031) | 0.0003** |
| Sulcal basin area | 0.922 (0.029) | 0.937 (0.010) | 0.2083 | 0.932 (0.021) | 0.927 (0.015) | 0.5456 |
| Sulcal depth | 0.923 (0.022) | 0.916 (0.014) | 0.4487 | 0.922 (0.023) | 0.924 (0.025) | 0.8448 |
| | Comparison between corresponding sulcal regions | | | Comparison between corresponding sulcal regions | | |
| Combined features | 0.774 (0.034) | 0.760 (0.015) | 0.3351 | 0.792 (0.028) | 0.743 (0.028) | 0.0008* |
| 3D position | 0.889 (0.019) | 0.840 (0.015) | <0.0001** | 0.889 (0.017) | 0.842 (0.023) | <0.0001** |
| Sulcal basin area | 0.832 (0.036) | 0.851 (0.017) | 0.1920 | 0.852 (0.028) | 0.825 (0.023) | 0.0357* |
| Sulcal depth | 0.935 (0.017) | 0.934 (0.009) | 0.9881 | 0.937 (0.019) | 0.924 (0.028) | 0.1956 |
| | Comparison of intersulcal relationships | | | Comparison of intersulcal relationships | | |
| Combined features | 0.822 (0.035) | 0.768 (0.021) | 0.0009* | 0.815 (0.033) | 0.768 (0.036) | 0.0059* |
| 3D position | 0.862 (0.032) | 0.798 (0.018) | <0.0001** | 0.852 (0.029) | 0.796 (0.029) | 0.0003** |
| Sulcal basin area | 0.944 (0.015) | 0.951 (0.007) | 0.2402 | 0.950 (0.013) | 0.952 (0.017) | 0.7291 |
| Sulcal depth | 0.921 (0.027) | 0.913 (0.013) | 0.4350 | 0.920 (0.024) | 0.922 (0.025) | 0.7942 |

Data: mean (standard deviation), *corrected $P \leq 0.05$ (uncorrected $P = 0.0141$), **corrected $P \leq 0.001$.

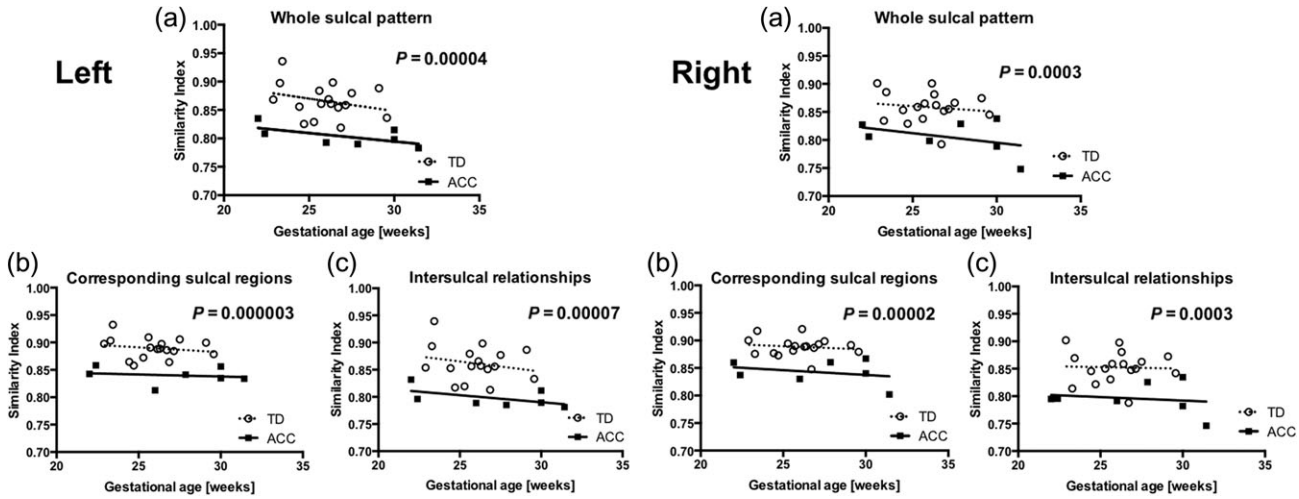


**Figure 4.** Distribution of SI. SI of sulcal position was analyzed in (*a*) whole sulcal pattern, (*b*) corresponding sulcal regions, and (*c*) intersulcal relationships in each case. SI is plotted as a function of gestational age. Distinct distribution between ACC and TD are illustrated in left and right hemispheres.

position according to the distribution of the SI of the TD fetuses. The ratio values for the sulcal position similarities over the whole-brain, between corresponding sulcal regions, and intersulcal relationships are shown for all individual fetuses with ACC in Table 2. Among sulcal features, comparison of corresponding sulcal region showed the most consistently lower percentile scores in ACC compared with TD brains in both hemispheres (Table 2). Most of the brains from fetuses with ACC were determined to have an abnormal corresponding sulcal position with a ratio of 0 (Left: ratio 0 for 6 of 7 cases and 0.059 for 1 case, Right: ratio 0 for 4 of 7 cases and 0.059 for 3 cases). Figure 5 shows histograms of the distribution of SI of corresponding sulcal position for the entire TD group and individual values for the fetuses with ACC, demonstrating that the distribution of ACC has minimal overlap with that of TD.

**Table 2** Ratio values (R) for the sulcal position similarities in fetuses with ACC

| ID | Left hemisphere | | | Right hemisphere | | |
|---|---|---|---|---|---|---|
| | R1 | R2 | R3 | R1 | R2 | R3 |
| ACC1 | 0.176 | 0 | 0 | 0.059 | 0.059 | 0.059 |
| ACC2 | 0 | 0.059 | 0.176 | 0.059 | 0 | 0.059 |
| ACC3 | 0 | 0 | 0 | 0.059 | 0 | 0.059 |
| ACC4 | 0 | 0 | 0 | 0.059 | 0.059 | 0.176 |
| ACC5 | 0 | 0 | 0 | 0.235 | 0.059 | 0.235 |
| ACC6 | 0 | 0 | 0 | 0 | 0 | 0 |
| ACC7 | 0 | 0 | 0 | 0 | 0 | 0 |

R1: Comparison of whole pattern, R2: Comparison between corresponding sulcal regions, R3: Comparison of intersulcal relationships.

### 3D GI of Fetuses with Agenesis of Corpus Callosum

GI of the 2 groups was plotted for each hemisphere as a function of gestational age (Fig. 6). We examined the differences between ACC and TD in each hemisphere using the *t*-test. This did not reveal any significant differences (Left: $P = 0.3368$, Right: $P = 0.3066$). The GI of TD fetuses appeared to have a steady increase over time, reflecting the increasing number and deepening of the sulci with development. As GI has been shown to be a function of gestational age, we created a linear regression model with interaction to fit to each group in each hemisphere. We tested if the models were different between groups.

There were no differences in the trajectories of GI between TD and ACC in analysis of each individual hemisphere: left hemisphere (slope TD: 0.0104, ACC: 0.0060, $P = 0.3798$) and right hemisphere (slope TD: 0.0121, ACC: 0.0066, $P = 0.2791$). Differences in slopes of each analysis did not reach statistical significance.

## Discussion

Our SI-based quantitative MRI analyses of fetal cerebral sulcal development showed that "isolated" ACC is associated with a broad alteration in cerebral sulcal development that can be detected in the second and third trimester. The absolute position and the relative intersulcal relationship of evolving sulci in both hemispheres were significantly different in fetuses with ACC compared with TD fetuses. Analysis of intersulcal relationships assures that these differences are not the product of variations in fetal brain size or alignment. Such differences in sulcation persisted during the observed period. These results confirm that even in the case of "isolated" ACC, there are more global alterations in cerebral development that are already present as early as the second trimester. These differences do not correspond to the delayed and immature patterns of sulcal folding and do not appear to "catch up" during the fetal period. In this study, SI-based novel quantitative sulcal pattern analysis detected aberrant sulcal development with a higher sensitivity than GI.

### SI-Based Quantitative Sulcal Pattern Analysis of Fetal Brain

Evaluation of cerebral development in living fetuses with ACC has significant clinical relevance as it may determine future neurodevelopmental outcomes of affected individuals. Typically, conventional fetal MRI is utilized to determine if there are additional associated brain anomalies with ACC such as neuronal migration anomalies that would influence the outcome (Neal et al. 2015). When conventional fetal MRI does not detect associated anomalies—as in the case of "isolated" ACC—the prediction

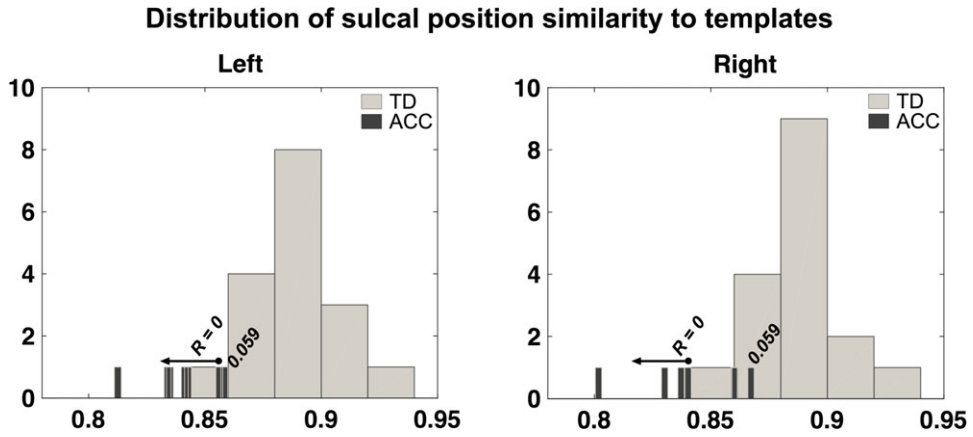


**Figure 5.** Distribution of sulcal position similarity to templates. Distribution of individual similarity indices (SI) of whole sulcal position pattern of ACC fetuses is compared with that of TD fetuses described in histograms. In fetuses with ACC, overall shifting to smaller similarity and large variation in SI is noted.

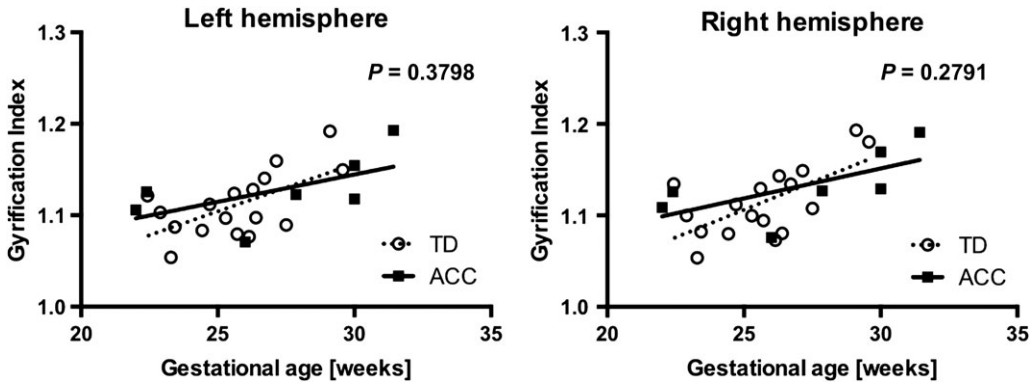


**Figure 6.** Developmental trajectory of GI. GI of ACC and TD groups is plotted for each hemisphere as a function of gestational age to compare the developmental trajectory of gyrification. Linear regression models of GI as a function of gestational age did not find significant differences between ACC (solid) and TD (dotted) groups.

of neurodevelopmental outcome is challenging. This may be partly explained by the low sensitivity of fetal MRI, as it does not detect all associated cerebral anomalies due to the small size of the fetal brain and limited resolution of fetal MRI (Mangione et al. 2011). It should be stressed out that the full extent of the abnormalities may not be present during the second trimester and at the time of fetal MRI study used in this study, prior to completion of gyrogenesis. We were not able to confirm the isolated nature of ACC in neonatal imaging, as not all cases had neonatal imaging. Yet, the study is considered to be relevant as we do not have access to such information at the time of prenatal diagnosis and counseling.

Prior studies have used qualitative visual assessment of the evolving patterns of sulci to estimate the gestational age of the fetal brain. This approach detected "delayed sulcation" in fetuses with ACC in the third trimester (Warren et al. 2010). However, our quantitative sulcal pattern analysis using 3 independent local sulcal features: 3D position, area, and depth of sulcal basin—detected significant group differences. The major feature driving the differences was the intersulcal geometric relationships characterizing interrelated sulcal arrangements and patterning in the left and right whole hemispheres. Sulcal position patterns evaluated by intersulcal relationships are less affected by confounding factors such as variable AC–PC alignment, the overall shape of brains, and the overall spatial shift of sulci in the case of complete ACC when both hemispheres appear to be pushed apart by the lack of connecting callosal tissue. These differences in sulcal pattern were persistent during the observed period (from 22 to 32 weeks of gestation) and did not "catch up" (Fig. 4). Therefore, by our measures, sulcal development in fetuses with ACC are aberrant rather than "delayed".

Using GI, we could not detect aberrant sulcal development in the second to third trimester fetuses with ACC. Large intragroup variations in sulcal development (Fig. 6) and low numbers of subjects likely contributed to the lack of statistical power. However, the lack of significance may also be due to the intrinsic limitation of GI. By definition, GI would sensitively detect sulcal aberrations when sulcal morphology is altered in sulcal basin area or depth. If sulcal aberrations are limited to the position of the sulci without affecting their depth or area, as shown in our analysis, GI may not detect such alterations. SI-based measures address these issues by measuring three independent sulcal features.

MRI-based sulcal pattern analysis on the fetal brains is not free from limitations. Among 32 TD and ACC fetal MRIs initially acquired, 8 MRI data were excluded mainly due to the failure of head motion correction and volume reconstruction and success rate for the processing was 75% (24/32). Future accelerations in image acquisition and improvements in postprocessing techniques are likely to increase success rates moving forward. Using MRI processing, identification of some early sulci lags behind histopathology due to the limitation of fetal MRI resolution, accuracy of cortical surface segmentation, and image smoothing

process (Chi et al. 1977; Garel et al. 2003; White et al. 2010; Rajagopalan et al. 2011). Smoothing could eliminate cortical folds that are less than 2 mm during the postprocessing, however, this smoothing was necessary to avoid noisy features and voxelized representation of the cortical plate surface. As we were able to quantify geometric features of major sulci, we believe that our approach is valid for assessment of the early emergence of these major sulci and their relationships. For more sensitive detection of the early sulcal appearance, advances in fetal MRI acquisitions with higher spatial resolution at equivalent signal to noise ratios without or minimizing motion degradation will be necessary.

## How Does Altered Callosal Connectivity Affect Gyral/Sulcal Development?

During the embryonic period, axonal development critically regulates gyral and sulcal development through various mechanisms. Organization of white matter connections influences the optimal cortical arealization, and, as a consequence, the resulting cortical folding patterns (Klyachko and Stevens 2003; Fischl et al. 2008). During development, axons terminating in the cortex, including those that arise from the contralateral cortex, influence gyrogenesis by regulating basal radial glial cell and basal intermediate progenitor proliferation (Sun and Hevner 2014) or by mechanistic tension for formulation of gyri (Van Essen 1997). Regional specific regulation in neuroprogenitor cell proliferation can influence regional gyral formation via differential tangential expansion by radial intercalation (Sekine et al. 2011; Striedter et al. 2015). Thalamocortical connections also influence neocortical arealization via regulation of various transcription factors in neuroprogenitor cells (Chou et al. 2013; Vue et al. 2013). Patients with complete or partial ACC have local and global alterations in white matter connections. Heterotopic aberrant callosal trajectories such as bundles of Probst and sigmoid-shaped bundles can be detected by diffusion MRI (Tovar-Moll et al. 2007, 2014; Wahl et al. 2009; Kasprian et al. 2013). Disrupted global organization of the whole-brain structural networks is seen in ACC (Owen et al. 2013; Jakab et al. 2015), which emerges as early as in fetal life (Kasprian et al. 2013; Jakab et al. 2015). It can be assumed that in fetuses with ACC, these changes in callosal and global white matter connections may also alter cortical arealization and thus positional organization of sulcal folds with similar mechanisms. Altered sulcal position in fetal brain may lay the foundation for altered cortical arealization that may result in cognitive and motor impairment in patients with ACC.

## Neuroembryology of Isolated Agenesis of Corpus Callosum

In all 7 cases of isolated ACC, we identified preserved anterior and posterior commissures (Supplementary Fig. 2*a*–*c*). Therefore, development of pathology may have occurred between 7 and 10 GW after anterior commissure is formed from lamina terminalis and before the first pioneering axon traverser the interhemispheric midline (Sarnat 2008). This finding is also consistent with former studies reporting preserved or enlarged anterior commissure in cases of ACC, possibly as a compensatory connection for interhemispheric processing in callosal agenesis (De Rosa 1992; Barr and Corballis 2002). Re-organization of cortical function may occur as one of subsequent developmental aberrations following such interhemispheric aberrant connections. As in this study, colpocephaly, dilatation of posterior lateral ventricles, may be observed in isolated ACC. Re-organization of primary visual field has been suggested by a prior functional MRI study (Bittar et al. 2000). These findings may suggest for re-organization of visual field may occur in association with alterations in occipital lobe gyrification and white matter connections.

## Does Altered Sulcal Development in "Isolated" Agenesis of Corpus Callosum Predict Future Neurodevelopment?

Absent or hypoplastic corpus callosum, which is the cardinal feature of ACC, has a broad influence on an affected individual's cognitive and behavioral function, as reviewed by Paul et al. 2007. Even in cases of "isolated" ACC, the nature and severity of neurodevelopmental impact has a broad spectrum (Fratelli et al. 2007; Chadie et al. 2008; Ghi et al. 2010; Mangione et al. 2011). In prenatal diagnosis, ACC is still considered to be "isolated" with associated features of colpocephaly and altered cingulate foldings because these are common features and not considered to add prognostic value. ACC will not be called "isolated" if there are associated cerebral anomalies such as polymicrogyria or schizencephaly (especially if they are broader anomalies), as they have additional prognostic value. Thus, anomalies in cerebral developmental may have more weight on determining neurodevelopmental function of affected person. In terms of cerebral development, this study proposes that "isolated" ACC in pure meaning may not exist and there are typically associated abnormalities in cortical folding.

Prior studies hypothesized that such cognitive and behavioral differences in individuals with ACC were the result of anomalies in axonal connections (Owen et al. 2013; Siffredi et al. 2013; Benezit et al. 2015; Jakab et al. 2015). This study adds the observation of aberrant gyral/sulcal development in fetuses with ACC (Figs 4 and 5). Importantly, both SIs and ratio values reflect measurable heterogeneity in sulcal development among ACC fetuses. Therefore, individual SI and ratio value may serve as novel biomarkers potentially associated with an individual's postnatal neurodevelopmental function. As this is an observation derived from small number of cases, the hypothesis needs to be tested in larger scale cohort in future prospective study with follow-up neurodevelopmental outcome data. In Figure 5, the gyral folding patterns in ACC were depicted to shift toward lower SI, with small overlap with that of TD.

Our study has limitations. First, the full distribution of SIs and ratio values in both ACC and TD groups is not yet fully explored given the small subject numbers in this pilot study. Larger fetal studies may further delineate their distribution and enable the ratio value to function as a "percentile" to tell where each individual's sulcal development lies compared to TD. To do so, multicenter recruitment will be necessary to recruit a sufficient number of these relatively rare fetal cases. Second, in this study, MR images were acquired in 3 institutions using different manufactures and magnet powers, which could lead to variations in image intensity range, tissue contrast, and consequent tissue segmentation. While the sequences may have slight differences in how they are acquiring the MRI signal, the end images among different manufactures are extremely similar. This is the case for the ultrafast T2 sequence used in this study, which has a different name depending on the manufacture (HASTE = Siemens, SSFSE = GE, SSTSE = Philips). These are widely considered equivalent, resulting in similar image quality. Additionally, our cortical plate segmentation was not an intensity-based automatic procedure, which is sensitive to tissue contrast, but was visually examined and edited based on anatomical knowledge of the fetal brain. Moreover, while a volumetric measurement such as cortical thickness depends on reliable tissue contrast of the inner and

outer cortical boundaries, the cortical folding shape measurement is relatively less influenced by tissue intensity contrast, though differences might increase noise and reduce statistical power. Finally, not all cases (especially, those that were retrospectively identified) in this study had postnatal MRI and clinical follow-up to confirm the isolated nature of their ACC and to determine their neurodevelopmental outcomes. Postnatal follow-up is ongoing for the cases recruited prospectively. A future study determining the association between such sulcal alterations and postnatal neurodevelopmental outcome is ongoing.

This study has shown that SI-based sulcal pattern analysis is valid to detect consistent sulcal pattern aberrations between groups. For a larger scale fetal study, multi-center recruitment will be necessary to recruit a sufficient number of these relatively rare fetal cases. This study has established the foundation for future larger scale collaborative studies.

## Supplementary Material

Supplementary data are available at *Cerebral Cortex* online.

## Funding

Research reported in this publication was supported by National Institutes of Health (K23HD079605-02, 1R01EB017337-01, 1U01HD087211-01), the Eunice Kennedy Shriver National Institute of Child Health & Human Development of the National Institutes of Health (R21HD083956), the Susan Saltonstall Foundation, Boston Children's Hospital Faculty Career Development Award, and the Mend a Heart Foundation. Funding from K12NS079414 from the National Institute of Neurological Disorders and Stroke and a Scholar Award from the Pediatric Heart Network (PHN) supported by the National Heart, Lung, and Blood Institute of the National Institutes of Health (U10HL068270) is acknowledged.

## Notes

The authors thank Michael Stanley and Annie Felhofer for their help with the post-acquisition segmentation of fetal brain MRI, Drs. SuMon Thwe, Cristin Wehbe, Ada Taymoori and Treeva Jassim for helping identification and recruitment of the participants, Rosemary Truong, Nancy Davis and Kristen Newell to coordinate research MRI studies, Theresa Peterson, Roanna Forman and John Gonsalves for research administrative supports. *Conflict of Interest*: None declared.

## References

Armstrong E, Schleicher A, Omran H, Curtis M, Zilles K. 1995. The ontogeny of human gyrification. Cereb Cortex. 5:56–63.

Bae BI, Tietjen I, Atabay KD, Evrony GD, Johnson MB, Asare E, Wang PP, Murayama AY, Im K, Lisgo SN, et al. 2014. Evolutionarily dynamic alternative splicing of GPR56 regulates regional cerebral cortical patterning. Science. 343: 764–768.

Barkovich AJ, Guerrini R, Kuzniecky RI, Jackson GD, Dobyns WB. 2012. A developmental and genetic classification for malformations of cortical development: update 2012. Brain. 135: 1348–1369.

Barr MS, Corballis MC. 2002. The role of the anterior commissure in callosal agenesis. Neuropsychology. 16:459–471.

Benezit A, Hertz-Pannier L, Dehaene-Lambertz G, Monzalvo K, Germanaud D, Duclap D, Guevara P, Mangin JF, Poupon C, Moutard ML, et al. 2015. Organising white matter in a brain without corpus callosum fibres. Cortex. 63:155–171.

Benjamini Y, Hochberg Y. 1995. Controlling the false discovery rate: a practical and powerful approach to multiple testing. J R Stat Soc B. 57:289–300.

Bittar RG, Ptito A, Dumoulin SO, Andermann F, Reutens DC. 2000. Reorganisation of the visual cortex in callosal agenesis and colpocephaly. J Clin Neurosci. 7:13–15.

Bloom JS, Hynd GW. 2005. The role of the corpus callosum in interhemispheric transfer of information: excitation or inhibition? Neuropsychol Rev. 15:59–71.

Chadie A, Radi S, Trestard L, Charollais A, Eurin D, Verspyck E, Marret S. 2008. Neurodevelopmental outcome in prenatally diagnosed isolated agenesis of the corpus callosum. Acta Paediatr. 97:420–424.

Chi JG, Dooling EC, Gilles FH. 1977. Gyral development of the human brain. Ann Neurol. 1:86–93.

Chou SJ, Babot Z, Leingartner A, Studer M, Nakagawa Y, O'Leary DD. 2013. Geniculocortical input drives genetic distinctions between primary and higher-order visual areas. Science. 340:1239–1242.

Chung MK, Robbins SM, Dalton KM, Davidson RJ, Alexander AL, Evans AC. 2005. Cortical thickness analysis in autism with heat kernel smoothing. NeuroImage. 25:1256–1265.

Clouchoux C, du Plessis AJ, Bouyssi-Kobar M, Tworetzky W, McElhinney DB, Brown DW, Gholipour A, Kudelski D, Warfield SK, McCarter RJ, et al. 2013. Delayed cortical development in fetuses with complex congenital heart disease. Cereb Cortex. 23:2932–2943.

Cox RW. 2012. AFNI: what a long strange trip it's been. NeuroImage. 62:743–747.

Cykowski MD, Kochunov PV, Ingham RJ, Ingham JC, Mangin JF, Riviere D, Lancaster JL, Fox PT. 2008. Perisylvian sulcal morphology and cerebral asymmetry patterns in adults who stutter. Cereb Cortex. 18:571–583.

D'Antonio F, Pagani G, Familiari A, Khalil A, Sagies TL, Malinger G, Leibovitz Z, Garel C, Moutard ML, Pilu G, et al. 2016. Outcomes associated with isolated agenesis of the corpus callosum: a meta-analysis. Pediatrics. 138:e20160445.

De Rosa MJ, Secor DL, Barsom M, Fisher RS, Vinters HV. 1992. Neuropathologic findings in surgically treated hemimegalencephaly: immunohistochemical, morphometric, and ultrastructural study. Acta Neuropathol. 84:250–260.

Derrfuss J, Brass M, von Cramon DY, Lohmann G, Amunts K. 2009. Neural activations at the junction of the inferior frontal sulcus and the inferior precentral sulcus: interindividual variability, reliability, and association with sulcal morphology. Hum Brain Mapp. 30:299–311.

Fischl B, Rajendran N, Busa E, Augustinack J, Hinds O, Yeo BT, Mohlberg H, Amunts K, Zilles K. 2008. Cortical folding patterns and predicting cytoarchitecture. Cereb Cortex. 18: 1973–1980.

Fratelli N, Papageorghiou AT, Prefumo F, Bakalis S, Homfray T, Thilaganathan B. 2007. Outcome of prenatally diagnosed agenesis of the corpus callosum. Prenat Diagn. 27:512–517.

Garel C, Chantrel E, Elmaleh M, Brisse H, Sebag G. 2003. Fetal MRI: normal gestational landmarks for cerebral biometry, gyration and myelination. Child's Nerv Syst. 19:422–425.

Genovese CR, Lazar NA, Nichols T. 2002. Thresholding of statistical maps in functional neuroimaging using the false discovery rate. NeuroImage. 15:870–878.

Ghi T, Carletti A, Contro E, Cera E, Falco P, Tagliavini G, Michelacci L, Tani G, Youssef A, Bonasoni P, et al. 2010. Prenatal diagnosis and outcome of partial agenesis and hypoplasia of the corpus callosum. Ultrasound Obstetr Gynecol. 35:35–41.

Im K, Guimaraes A, Kim Y, Cottrill E, Gagoski B, Rollins C, Ortinau C, Yang E, Grant PE. 2017. Quantitative folding pattern analysis of early primary sulci in human fetuses with brain abnormalities. AJNR Am J Neuroradiol. 38:1449–1455.

Im K, Jo HJ, Mangin JF, Evans AC, Kim SI, Lee JM. 2010. Spatial distribution of deep sulcal landmarks and hemispherical asymmetry on the cortical surface. Cereb Cortex. 20:602–611.

Im K, Pienaar R, Lee JM, Seong JK, Choi YY, Lee KH, Grant PE. 2011. Quantitative comparison and analysis of sulcal patterns using sulcal graph matching: a twin study. NeuroImage. 57:1077–1086.

Im K, Pienaar R, Paldino MJ, Gaab N, Galaburda AM, Grant PE. 2013. Quantification and discrimination of abnormal sulcal patterns in polymicrogyria. Cereb Cortex. 23:3007–3015.

Im K, Raschle NM, Smith SA, Ellen Grant P, Gaab N. 2016. Atypical Sulcal Pattern in Children with Developmental Dyslexia and At-Risk Kindergarteners. Cereb Cortex. 26:1138–1148.

Jakab A, Kasprian G, Schwartz E, Gruber GM, Mitter C, Prayer D, Schopf V, Langs G. 2015. Disrupted developmental organization of the structural connectome in fetuses with corpus callosum agenesis. NeuroImage. 111:277–288.

Jeret JS, Serur D, Wisniewski KE, Lubin RA. 1987. Clinicopathological findings associated with agenesis of the corpus callosum. Brain Dev. 9:255–264.

Kasprian G, Brugger PC, Schopf V, Mitter C, Weber M, Hainfellner JA, Prayer D. 2013. Assessing prenatal white matter connectivity in commissural agenesis. Brain. 136:168–179.

Kim H, Bernasconi N, Bernhardt B, Colliot O, Bernasconi A. 2008. Basal temporal sulcal morphology in healthy controls and patients with temporal lobe epilepsy. Neurology. 70: 2159–2165.

Klyachko VA, Stevens CF. 2003. Connectivity optimization and the positioning of cortical areas. Proc Natl Acad Sci USA. 100:7937–7941.

Kuklisova-Murgasova M, Quaghebeur G, Rutherford MA, Hajnal JV, Schnabel JA. 2012. Reconstruction of fetal brain MRI with intensity matching and complete outlier removal. Med Image Anal. 16:1550–1564.

Lefevre J, Germanaud D, Dubois J, Rousseau F, de Macedo Santos I, Angleys H, Mangin JF, Huppi PS, Girard N, De Guio F. 2015. Are developmental trajectories of cortical folding comparable between cross-sectional datasets of fetuses and preterm newborns? Cereb Cortex. 26:3023–3035.

Leordeanu M, Hebert M. 2005 A spectral technique for correspondence problems using pairwise constraints. ICCV '05: Proceedings of the Tenth IEEE International Conference on Computer Vision. Washington, DC: IEEE Computer Society. p. 1482–1489.

Lohmann G, von Cramon DY. 2000. Automatic labelling of the human cortical surface using sulcal basins. Med Image Anal. 4:179–188.

Mangione R, Fries N, Godard P, Capron C, Mirlesse V, Lacombe D, Duyme M. 2011. Neurodevelopmental outcome following prenatal diagnosis of an isolated anomaly of the corpus callosum. Ultrasound obstetr Gynecol. 37:290–295.

Molko N, Cachia A, Riviere D, Mangin JF, Bruandet M, Le Bihan D, Cohen L, Dehaene S. 2003. Functional and structural alterations of the intraparietal sulcus in a developmental dyscalculia of genetic origin. Neuron. 40:847–858.

Nakamura M, Nestor PG, McCarley RW, Levitt JJ, Hsu L, Kawashima T, Niznikiewicz M, Shenton ME. 2007. Altered orbitofrontal sulcogyral pattern in schizophrenia. Brain. 130: 693–707.

Neal JB, Filippi CG, Mayeux R. 2015. Morphometric variability of neuroimaging features in children with agenesis of the corpus callosum. BMC Neurol. 15:116.

Owen JP, Li YO, Ziv E, Strominger Z, Gold J, Bukhpun P, Wakahiro M, Friedman EJ, Sherr EH, Mukherjee P. 2013. The structural connectome of the human brain in agenesis of the corpus callosum. NeuroImage. 70:340–355.

Paul LK, Brown WS, Adolphs R, Tyszka JM, Richards LJ, Mukherjee P, Sherr EH. 2007. Agenesis of the corpus callosum: genetic, developmental and functional aspects of connectivity. Nat Rev Neurosci. 8:287–299.

Rajagopalan V, Scott J, Habas PA, Kim K, Corbett-Detig J, Rousseau F, Barkovich AJ, Glenn OA, Studholme C. 2011. Local tissue growth patterns underlying normal fetal human brain gyrification quantified in utero. J Neurosci. 31: 2878–2887.

Richards LJ, Plachez C, Ren T. 2004. Mechanisms regulating the development of the corpus callosum and its agenesis in mouse and human. Clin Genet. 66:276–289.

Rimrodt SL, Peterson DJ, Denckla MB, Kaufmann WE, Cutting LE. 2010. White matter microstructural differences linked to left perisylvian language network in children with dyslexia. Cortex. 46:739–749.

Sarnat HB. 2008. Embryology and malformations of the forebrain commissures. Handb Clin Neurol. 87:67–87.

Schaer M, Cuadra MB, Tamarit L, Lazeyras F, Eliez S, Thiran JP. 2008. A surface-based approach to quantify local cortical gyrification. IEEE Trans Med Imaging. 27:161–170.

Sekine K, Honda T, Kawauchi T, Kubo K, Nakajima K. 2011. The outermost region of the developing cortical plate is crucial for both the switch of the radial migration mode and the Dab1-dependent "inside-out" lamination in the neocortex. J Neurosci. 31:9426–9439.

Serag A, Aljabar P, Ball G, Counsell SJ, Boardman JP, Rutherford MA, Edwards AD, Hajnal JV, Rueckert D. 2012. Construction of a consistent high-definition spatio-temporal atlas of the developing brain using adaptive kernel regression. NeuroImage. 59:2255–2265.

Shim G, Jung WH, Choi JS, Jung MH, Jang JH, Park JY, Choi CH, Kang DH, Kwon JS. 2009. Reduced cortical folding of the anterior cingulate cortex in obsessive-compulsive disorder. J Psychiatry Neurosci. 34:443–449.

Shimony JS, Smyser CD, Wideman G, Alexopoulos D, Hill J, Harwell J, Dierker D, Van Essen DC, Inder TE, Neil JJ. 2016. Comparison of cortical folding measures for evaluation of developing human brain. NeuroImage. 125:780–790.

Siffredi V, Anderson V, Leventer RJ, Spencer-Smith MM. 2013. Neuropsychological profile of agenesis of the corpus callosum: a systematic review. Dev Neuropsychol. 38:36–57.

Striedter GF, Srinivasan S, Monuki ES. 2015. Cortical folding: when, where, how, and why? Annu Rev Neurosci. 38: 291–307.

Sun T, Hevner RF. 2014. Growth and folding of the mammalian cerebral cortex: from molecules to malformations. Nat Rev Neurosci. 15:217–232.

Tang PH, Bartha AI, Norton ME, Barkovich AJ, Sherr EH, Glenn OA. 2009. Agenesis of the corpus callosum: an MR imaging analysis of associated abnormalities in the fetus. AJNR Am J Neuroradiol. 30:257–263.

Tovar-Moll F, Moll J, de Oliveira-Souza R, Bramati I, Andreiuolo PA, Lent R. 2007. Neuroplasticity in human callosal dysgenesis: a diffusion tensor imaging study. Cereb Cortex. 17:531–541.

Tovar-Moll F, Monteiro M, Andrade J, Bramati IE, Vianna-Barbosa R, Marins T, Rodrigues E, Dantas N, Behrens TE, de Oliveira-Souza R, et al. 2014. Structural and functional brain rewiring clarifies preserved interhemispheric transfer in humans born without the corpus callosum. Proc Natl Acad Sci U SA. 111:7843–7848.

Van Essen DC. 1997. A tension-based theory of morphogenesis and compact wiring in the central nervous system. Nature. 385:313–318.

Vandermosten M, Boets B, Poelmans H, Sunaert S, Wouters J, Ghesquiere P. 2012. A tractography study in dyslexia: neuroanatomic correlates of orthographic, phonological and speech processing. Brain. 135:935–948.

Vue TY, Lee M, Tan YE, Werkhoven Z, Wang L, Nakagawa Y. 2013. Thalamic control of neocortical area formation in mice. J Neurosci. 33:8442–8453.

Wahl M, Strominger Z, Jeremy RJ, Barkovich AJ, Wakahiro M, Sherr EH, Mukherjee P. 2009. Variability of homotopic and heterotopic callosal connectivity in partial agenesis of the corpus callosum: a 3 T diffusion tensor imaging and Q-ball tractography study. AJNR Am J Neuroradiol. 30:282–289.

Warren DJ, Connolly DJ, Griffiths PD. 2010. Assessment of sulcation of the fetal brain in cases of isolated agenesis of the corpus callosum using in utero MR imaging. AJNR Am J Neuroradiol. 31:1085–1090.

White T, Su S, Schmidt M, Kao CY, Sapiro G. 2010. The development of gyrification in childhood and adolescence. Brain Cogn. 72:36–45.

Zilles K, Armstrong E, Schleicher A, Kretschmann HJ. 1988. The human pattern of gyrification in the cerebral cortex. Anat Embryol (Berl). 179:173–179.